JMEPEG
https://doi.org/10.1007/s11665-024-09296-8

1059-9495/$19.00

ORIGINAL RESEARCH ARTICLE

Preparation and Flame Ablation Resistance of Al/Zn/Cu-Incorporated Yttria Partially Stabilized Zirconia Coating

Yuxing Fan, Haoliang Tian, Shuaishuai Zhu, Cong Fang, and Baosen Zhang

Submitted: 13 November 2023 / Revised: 26 December 2023 / Accepted: 2 February 2024

Al/Zn/Cu-incorporated yttria partially stabilized zirconia (YSZ) coating was prepared on carbon fiber-reinforced polyimide sheets by the detonation spraying process to enhance the heat resistance of resin composites. The microstructure and phase composition of the coatings were analyzed by using XRD, SEM and XPS. The flame ablation platform was used to analyze the coating's thermal protection capabilities. The coating failure process and the protection mechanisms of Al, Zn, and Cu metals were examined and described. The results show that it is possible to prepare dense coatings with good bonding between layers using detonation spraying. In the working layer, both Al and Zn additive phases were oxidized to some extent and the oxidation products were Al_2O_3 and ZnO. Al and Zn play the role of melting and heat absorption to lower the temperature, and the newly generated Al_2O_3, ZnO and CuO under the high temperature play the role of repairing the cracks in the coatings, slowing down the growth of the thermally grown oxide (TGO) as well as the role of heat insulation.

Keywords aerospace, detonation spraying, flame ablation, thermal spray, YSZ

1. Introduction

Currently, the rapid development of aerospace is driving composite materials toward high performance, low cost, and multifunction by putting forward ever-higher requirements (Ref 1). One of the most commonly used materials in aviation (Ref 2) is resin-based composites, which are composed of fiber-reinforced resins (Ref 3, 4). Although resin-based composites exhibit excellent mechanical and chemical resistance, they still have major shortcomings in terms of thermal and electrical properties (Ref 5-7). These issues will affect its wide application in the aerospace field (Ref 8-10).

In recent years, researchers have attempted to prepare coatings on resin-based composites using various spraying methods to improve their thermal and electrical properties. These coating methods are: thermal spraying (Ref 11), cold spraying (Ref 12), physical vapor deposition (PVD), chemical vapor deposition (CVD), and electroplating (Ref 13). The thermal spraying process has the advantages of economy, controllability, and a wide range of applications (Ref 14). Therefore, it is currently the main method for preparing coatings on the surface of resin-based composites (Ref 15). In the study of the metallization of resin matrix composites using various thermal spraying processes, the explosion spraying process has the best overall performance (Ref 16). In comparison to plasma spraying, the explosion spraying process results in resin matrix composites that are not degraded by high temperatures (Ref 17). Compared to flame spraying, explosion spraying has a higher powder traveling speed, which affects the overall quality of the coating (Ref 18).

The choice of coating system has a significant impact on the thermal performance enhancement of resin matrix composites. The selection of bonding layer composition needs to take into account factors such as its melting temperature and thermal spray expansion coefficient, and the most widely used methods are single or proportional mixes of metal coatings such as Al, Zn, and Cu (Ref 19, 20). In order to further improve the bonding ability between the metal coating and the resin matrix, researchers have used methods such as surface roughening (Ref 16), surface doping with metal powders (Ref 21), or the use of sprayed powders containing resin additives (Ref 22) to moderate the thermodynamic differences between the metal coating and the resin-based material. In addition, the proper spraying process parameters are one of the most important factors influencing the quality of the substrate (Ref 23). The presence of an intermediate layer is also necessary for the subsequent ceramic top layer that needs to be sprayed. The spraying of ceramic materials often requires the use of higher spray power and lower spray distances, so that the spraying of ceramic layers will result in a higher heat input (Ref 24). A three-layer coating system (low melting point metal layer + high temperature alloy layer + ceramic layer) mitigates the thermal damage to the resin-based substrate when spraying the top layer compared to a two-layer coating system (metal layer + ceramic layer) (Ref 25). The three-layer coating

Yuxing Fan, Shuaishuai Zhu, Cong Fang, and **Baosen Zhang**, School of Materials Science and Engineering, Nanjing Institute of Technology, Nanjing 211167, China; and Jiangsu Key Laboratory of Advanced Structural Materials and Application Technology, Nanjing 211167, China; and **Haoliang Tian**, Aviation Key Laboratory of Science and Technology on Advanced Corrosion and Protection for Aviation Material Beijing, Beijing Institute of Aeronautical Materials, Beijing 100095, China. Contact e-mails: haoliangtian@163.com and baosenzhang@njit.edu.cn.

Published online: 13 March 2024

system also provides layer-by-layer relief of thermal stresses at high temperatures, avoiding high stress concentrations in the coating (Ref 26).

Yttria Partially Stabilized Zirconia (YSZ) has been used as a heat resistant ceramic layer due to its low thermal conductivity at high temperatures. Existing research has been directed towards the use of rare earth oxides to stabilize zirconia to enhance its stability at high temperatures (Ref 27), while less research has been conducted on the introduction of the ablative cooling component of ablative coatings into ceramic thermal barrier coatings to form a composite thermal protective coating (Ref 22). A single thermal barrier coating is often prone to peeling off and failing under high-temperature service, while ablative coatings often need to be prepared thicker in order to meet the service standard (Ref 28, 29). Therefore, the introduction of the ablative phase in the thermal barrier coating can provide a new idea to solve the thermal protection of resin-based composite materials.

In this study, a ceramic matrix composite thermal protection coating was prepared on a polyimide substrate using the detonation spraying process. The structure, morphology, and ablation resistance of the YSZ coatings with low-melting-point metals (Al, Zn, and Cu) and pure YSZ coatings were investigated and compared to determine the effect of low melting point metals (Al, Zn, and Cu) on the coating's ablation resistance and failure mechanism.

2. Materials and Methods

2.1 Materials and Coating Deposition Methods

In this experiment, detonation spraying was used to prepare an Al/Zn/Cu-incorporated YSZ-based composite coating (called S1) on a carbon fiber-reinforced polyimide resin matrix. There were three different layers in S1 coating: a bonding layer, a transition layer, and a protective coating. Figure 1 shows the schematic representation of the coating's structure and the schematic diagram of detonation spraying. It was made up of four layers, which were Al/Zn/Cu-incorporated YSZ, NiCoCrAlYTa, Al, and polyimide composite, stacked from top to bottom. YSZ was the working layer that prevented perspiration, NiCoCrAlYTa was the transition layer, Al was the metal bonding layer, and the substrate was made of polyimide composite. A double-layer thermal barrier coating (named S2) comprising YSZ (unadulterated) and Al was prepared experimentally for comparison with the S1 coating in order to assess its ablation resistance against the traditional YSZ coating.

In this experiment, YSZ (204B Metco), phenolic resin, Al, Zn, Cu, and SiO_2 were utilized as raw materials to create ceramic composite powders using the solid phase synthesis method. Following their ball milling, mixing, drying, and sieving, these six raw materials were weighed in accordance with the chemical composition ratios listed in Table 1. An atomizing granulator was used for spray granulation, and the granulated powder was sieved to produce sprayed powder with particles smaller than 50 μm. NiCoCrAlYTa is the substance used in the intermediate layer (Amdry 997, Sulzer Metco). The powder's particle diameter is between 5 and 35 μm, and Table 2 displays its chemical composition. After being mechanically combined in a 49:1 ratio with aluminum and polyimide powders, the bottom powder was sieved through a 180-mesh screen. The Beijing Institute of Aerospace Materials supplied carbon fiber-reinforced polyimide composite panels with a glass transition temperature of 397 °C.

To improve the bonding between the sprayed particles and the matrix, sandblasting was used to roughen the surface of the composite. Corundum sand with a particle size of 100 mesh was chosen as the material to be blasted. The parameters for the sandblasting were as follows: 0.3 MPa of pressure, 60° of angle, 160 mm of distance, and 70 seconds of time. The detonation spraying process is used to process each layer of the composite coating. Table 3 displays the parameters of this process.

2.2 Flame Ablation Test

Ablation experiments were carried out using a mixture of oxygen and acetylene. The flame temperature at the surface of the coating was measured using a thermocouple located at the center region of the ablation on the sample surface. During the test, the temperature was increased from room temperature to 800 ± 20 °C in 10 s and then held at the peak temperature for another 300 s. The flame was then extinguished and the sample was cooled naturally to room temperature. Figure 2 shows the schematic diagram of the ablation experiment.

2.3 Evaluation of Coating Properties and Characterizations

Powder x-ray diffraction (XRD, Rigaku Ultima IV) was employed to identify the phase structure of the samples using Cu-Kα radiation (λ = 0.15406 nm), with a scan rate of 10°/min from 10 to 90°, and it was operated at an accelerating voltage of 40 kV and an emission current of 50 mA. The surface morphologies and the cross-sectional microstructures of the samples were investigated by scanning electron microscope (SEM, JSM-6360LV), and the distributions of elements were analyzed by means of energy dispersive spectroscopy (EDS). Through the method of image quantitative analysis, the cross-sectional morphology of the coating was analyzed by ImageJ software. After the cross-sectional SEM image of the coating was transformed into a grayscale image, 25 sections at different positions were selected. After the porosity was obtained by software analysis, the average

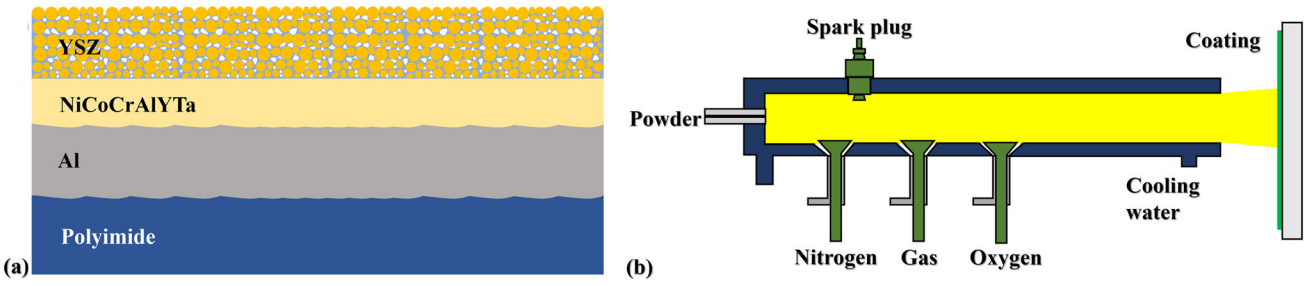

Fig. 1 (a) Schematic diagram of coating structure; (b) Schematic diagram of detonation Spraying

value was taken as the porosity value of the coating. YSZ composite powders were characterized by differential scanning calorimetry (DSC). x-ray photoelectron spectroscopy (XPS, Thermo Fisher K-Alpha +) was used to determine the valence states of Al, Cu and Zn. The XPS spectrum was recorded using monochromatic Al Kα x-ray source with a base pressure of 6.8×10^{-9} Torr. The survey spectrum was recorded with a pass energy of 100 eV. The XPS data were calibrated by using the adventitious C 1s signal at 284.8 eV as a reference, and the binding energy spectra were fitted by Avantage Software.

3. Results and Discussion

3.1 Characterization of Al/Zn/Cu-Incorporated YSZ Powders and Coatings

The S1 powder's micrographs are shown in Fig. 3(a). The two morphological characteristics of the powder were as follows: one of the particles presents a more spherical shape, while the other has an apple-like appearance due to an inwardly curved tip. During granulation, the location of the evaporation contacts inside the powder shifts, modifying the order of solidification. When the evaporation boundary moves outward, hollow spheres are created, and solid spherical particles are formed when it moves inward toward the powder's center (Ref 30). The majority of the powders had almost spherical shapes, which would make the thermal spraying process easier. EDS analyses of the S1 powder's composition are shown in Fig. 3(b). The content and testing methodology make it impossible to detect the addition of Zn, and Cu. XRD results of the S1 powders are demonstrated in Fig. 3(c), tetragonal phase (t'-YSZ) and a trace amount of monoclinic phase (m-YSZ) make up the majority of the YSZ powder (Ref 31). Two heat absorption peaks of YSZ powder are observed during the heating process from 23 to 800 °C, as shown in Fig. 3(d). These peaks sat 417.65 and 653.61 °C, which correspond to the melting and heat absorption reactions of the metals Zn and Al (Ref 32, 33). The cross section of the powder is observed by surface scanning using EDS in order to ascertain the distribution of each added phase in the original powder. The distribution of Zn elements in each added phase is the most uniform, which is consistent with the distribution of Zr and O elements as shown in Fig. 4. It is also found that Cu and Al show clear signs of segregation. This may be due to the difference in density and particle size of the powders, leading to uneven mixing and hence segregation during granulation.

Figure 5 shows the cross-sectional morphologies of the S1 and S2 coatings. It can be seen that the coating has no obvious layered structure, the powder melts fully, spreads evenly, and the interfaces are tightly bonded without an obvious oxidation interface, indicating that the high-speed particles impact the substrate or the pre-deposited layer during the detonation spraying process. In particular, attention is paid to the interface between the Al bottom layer and the composite matrix, and there is no burning phenomenon, microcracks or interface separation. As a pulsed spraying, the temperature of the substrate can be effectively controlled within a lower temperature range during the detonation spraying process, so that the damage to the substrate material is very small (Ref 34). In all samples of the composite coating, except for a few holes found between the middle layer and the surface layer, the layers are mechanically occluded and the interface is well bonded. The porosity of the surface working layer is 4.60% (S1) and 5.89%

Table 1 Chemical composition of S1 working layer material (wt.%)

	YSZ	Zn	Al	Cu	SiO_2	Resin liquid material
YSZ powder	90	2	2	2	2	2

Table 2 Chemical composition of S1 transition layer material (wt.%)

	Ni	Co	Cr	Al	Y	Ta
NiCoCrAlYTa	43.9	23	20	8.5	0.6	4

Table 3 Spraying process parameters

	Distance, mm	Frequency, shot/s	O_2/C_2H_2, %
Bond coat	160 ~ 180	2	24 ~ 28
Transition layer	160 ~ 180	2	30 ~ 34
Top layer	220 ~ 240	4	50 ~ 55

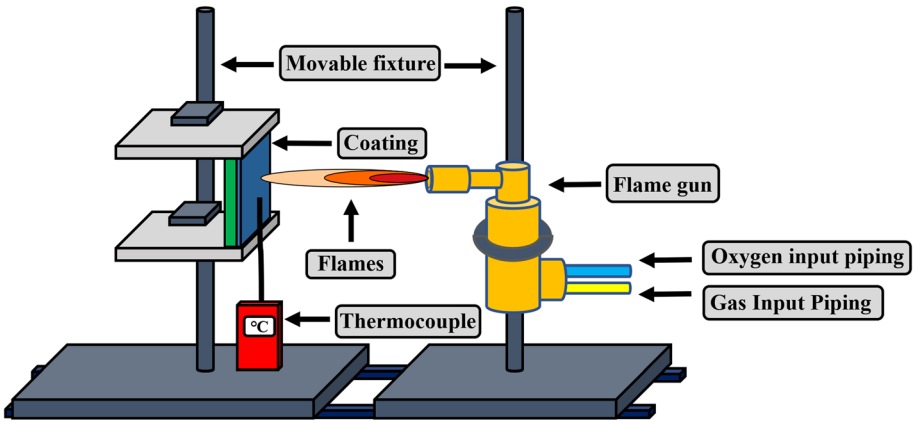

Fig. 2 Schematic diagram of ablation experiment

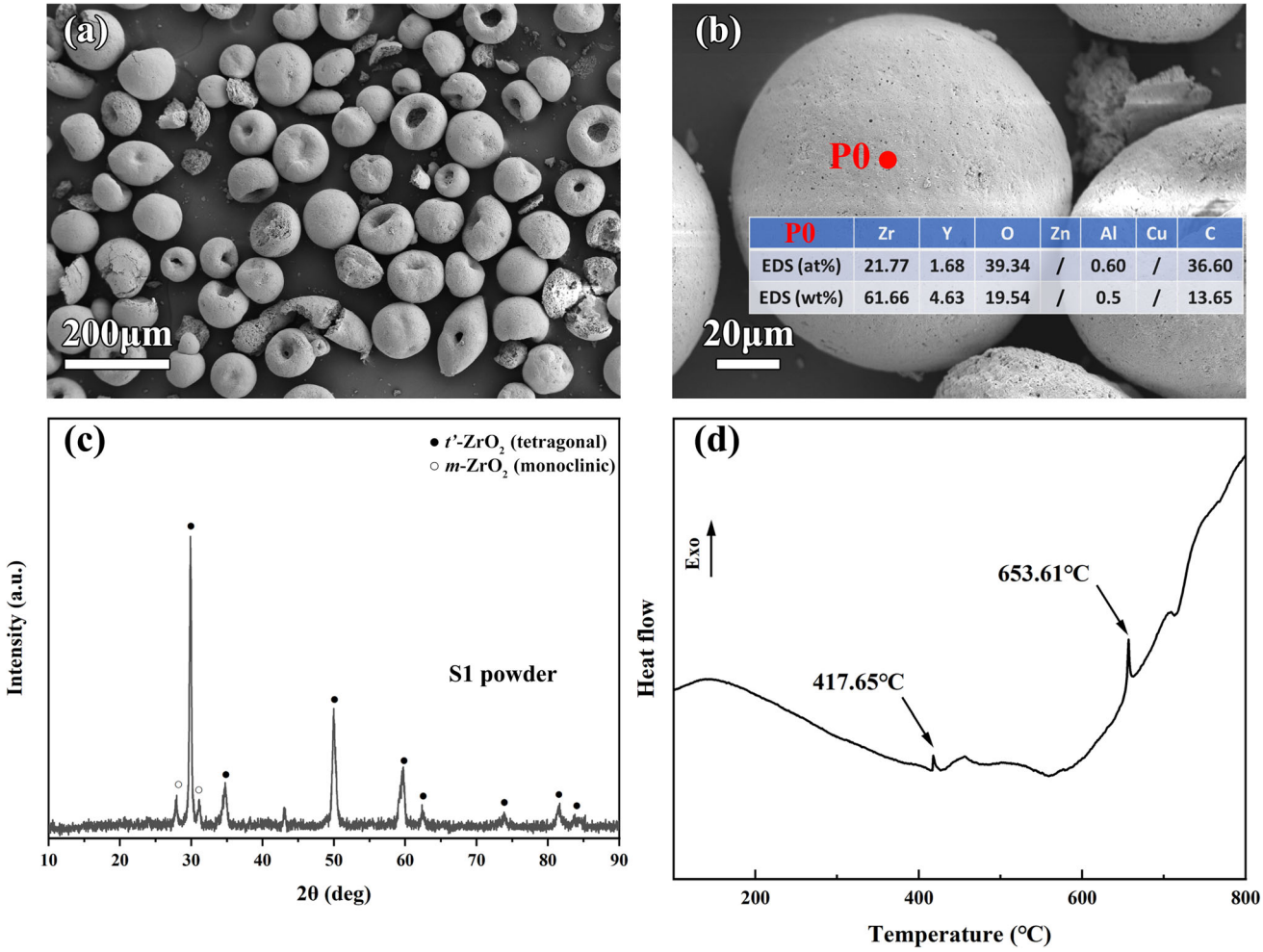

Fig. 3 (a) SEM micrographs of S1 powder; (b) EDS of S1 powder; (c) XRD patterns of S1 powder; (d) DSC of S1 powder

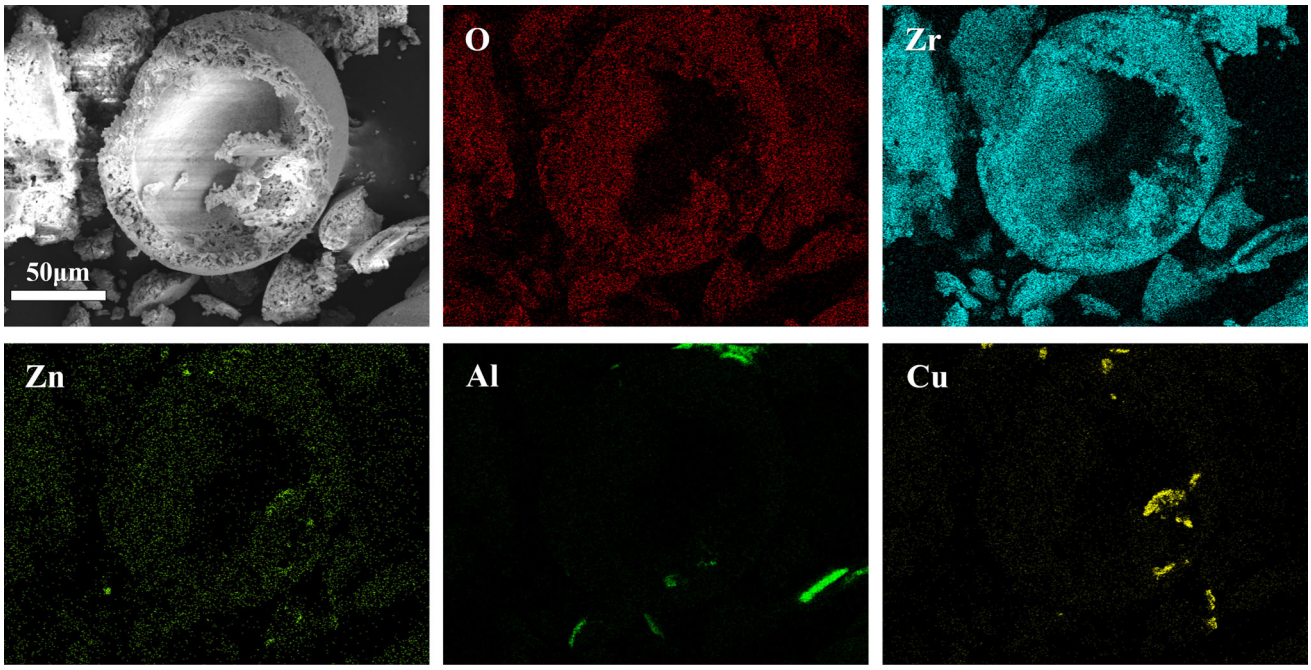

Fig. 4 S1 powder element surface distribution

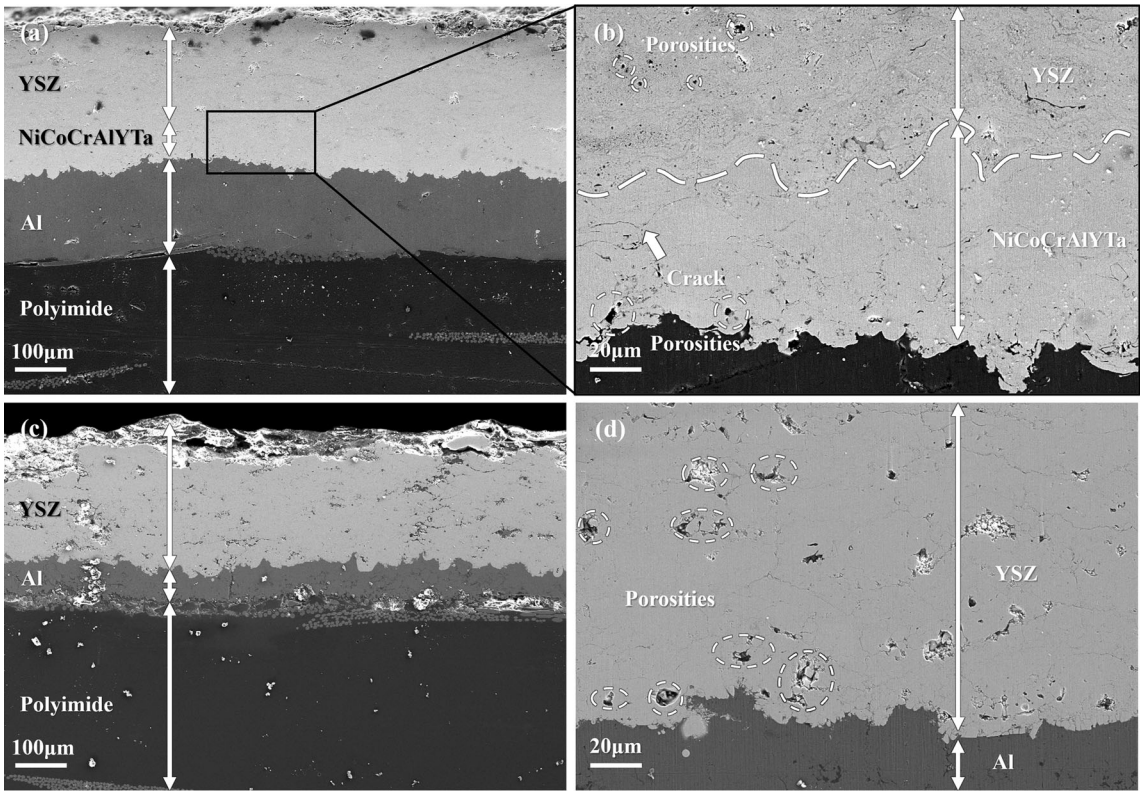

Fig. 5 (a) and (b) Cross-sectional morphologies of S1 coating; (c) and (d) Cross-sectional morphologies of S2 coating

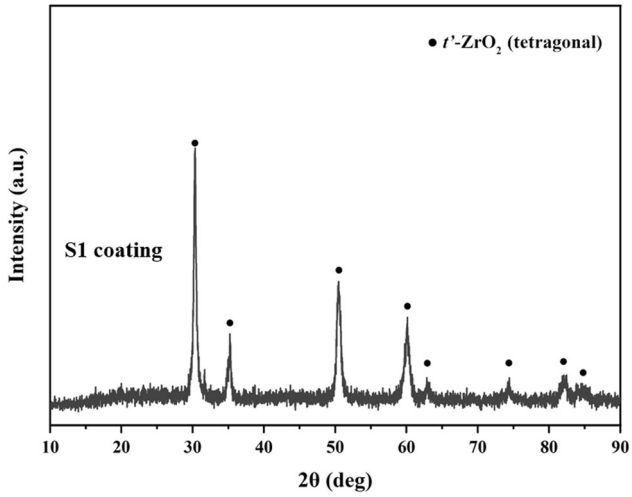

Fig. 6 XRD pattern of S1 coating's surface

(S2), respectively. The coating is denser compared to other thermal spraying methods (Ref 35). The metal doping in S1 made it denser.

The XRD patterns of the working layers in Fig. 6 show that the top layer of YSZ is mostly made up of t-YSZ. After the detonation spraying, the amount of m-YSZ in the YSZ decreased. Probably because of the rapid solidification and rapid cooling of YSZ splats after impacting the surface of the substrate during the spraying process, which limits the transition of phases (Ref 36). Figure 7 shows the element distribution of the working layer. After spraying, the Al, Cu and Zn additive phases are effectively distributed in the YSZ coating, and the uniform distribution of the additive phases will contribute to the overall thermal insulation of the coating.

3.2 Characterization of Coatings After Flame Ablation

As can be seen in Fig. 8(a), (b), (c), (d), (e), and (f), there are no obvious cracks or spalling under the macroscopic surface of the S1 and S2 coatings. The color of the ablated area of the S1 specimen is light gray, while the ablated area of the S2 specimen shows obvious black carbon deposits. In Fig. 8(b), and (c), it can be seen that the cracks in the edge region gradually increase from the side close to the substrate upwards due to the fact that the additive phase (Al, Cu and Zn) in the high temperature region can cause spilling out to the surface, which leading that the coating become loose. The peeling of the ceramic working layer are observed with exposure transition layer as shown in Fig. 8(c). The delamination location is between the Al metal bonding layer and the polyimide composite substrate. The difference in the coefficient of thermal expansion between the Al-metal layer and the resin-based composite also contributes to the peeling of the coating. (Ref 17). From Fig. 8(g), and (h), it can be seen that the peeling of the coating spread from the center region to the edges. The failure occurs at the center of the specimen, which may contribute to high thermal stress. Figure 8(d), (e), (i), and (j) reflects the oxygen content of the S1 and S2 coatings. The Al layer of the S1 coating has a lower oxygen content than the S2. This suggested that the S1 coating mitigates the oxidation of the Al layer, which would be delaying the generation of TGOs (Ref 37), and at the same time mitigates the oxidation of the substrate (Ref 17). In order to reveal the cooling mechanism of Al/Zn/Cu-incorporated YSZ based composite coating, the

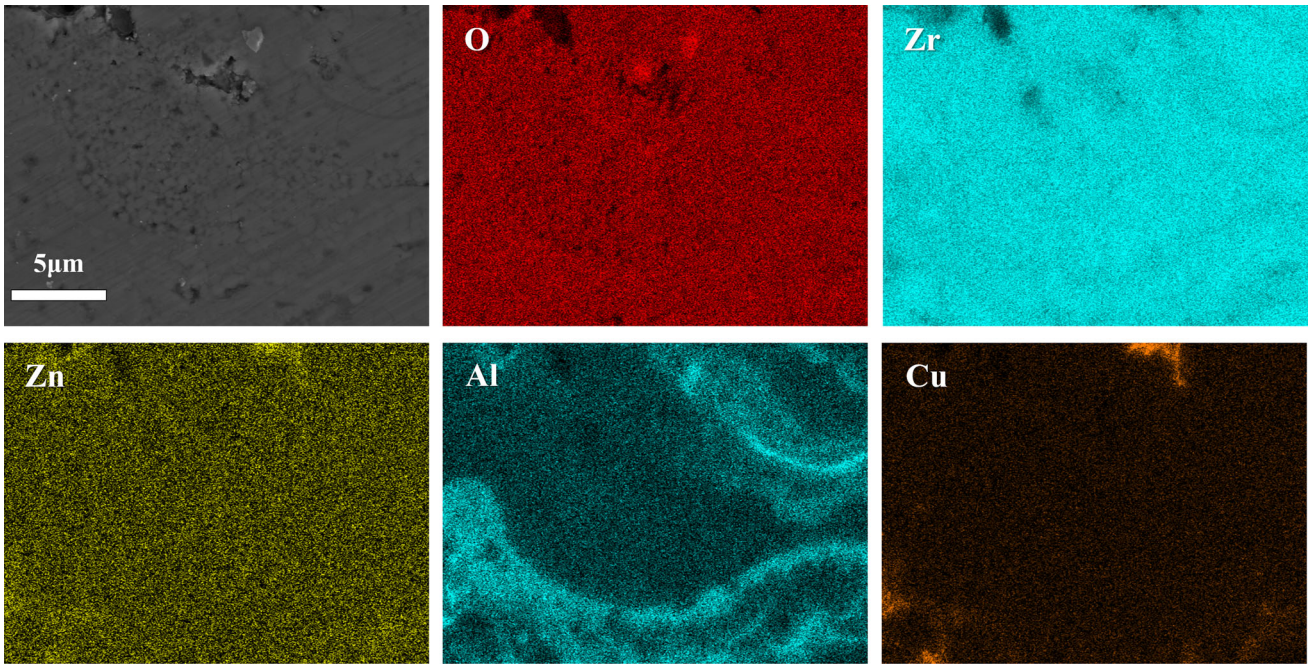

Fig. 7 EDS mapping results of S1 cross section

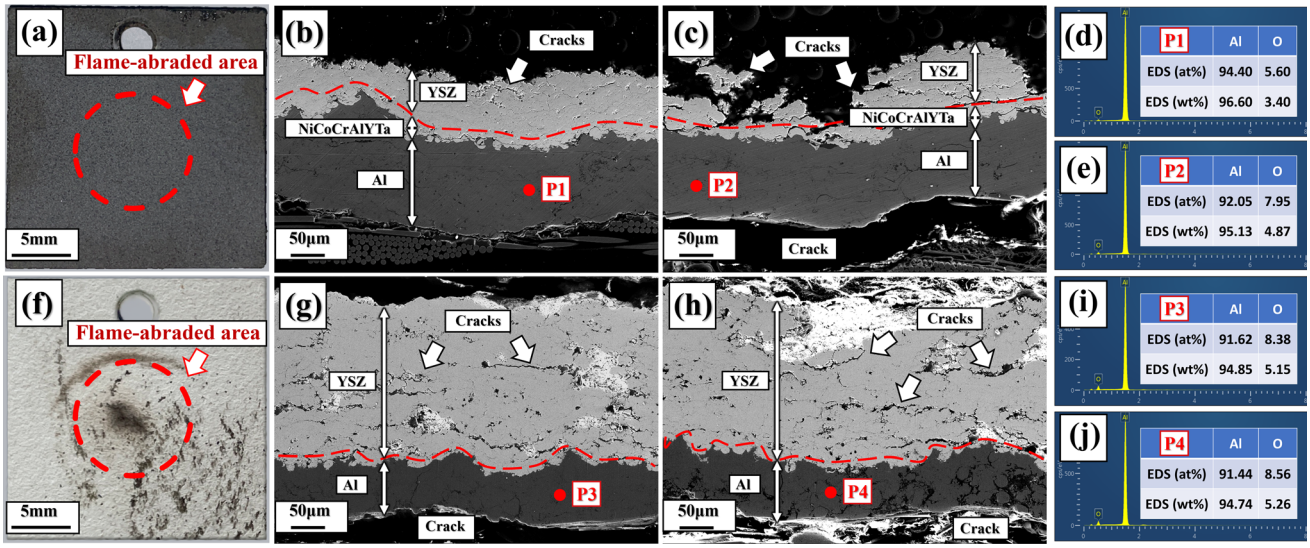

Fig. 8 Cross-section morphology of the coating after flame ablation (a) and (f) S1 and S2 coating ablated macroscopic morphology; (b) S1 coating edge area; (c) S1 coating center area; (g) S2 coating edge area; (h) S2 coating center area; (d), (e), (i) and (j) The composition of Al metal bonding layer by EDS

distribution and compositional changes of Al, Cu and Zn in the S1 coatings are investigated in the following section.

3.3 Cooling Mechanism of Al/Zn/Cu-Incorporated YSZ Based Composite Coating

From Fig. 9(b), it can be seen that part of the ceramic flake layer is still retained in the edge region of the thermal shock of the S1 coating. Compared with Fig. 9(a), there are obvious cracks and pits in the center region of the thermal shock. The metal additive phase overflows near the cracks and undergo a certain degree of oxidation. During the test, the temperature is gradually reduced from the center region of the thermal shock to the edge region. The shock effected by the flame also washed some liquefied metal to the edge. In the edge region of the thermal shock there is a partial overlap between the elements Al and O in some of the highlighted areas, so there is some oxidation of Al. In the central region of the ablation there is a partial overlap of the Cu and O elements with some highlighting areas, so there is some oxidation of Cu. Without considering the influence of defects (pores and humps) on the results of the elemental mapping of the concave and convex areas, it can be seen that Zn, as the lowest melting point and boiling point of the additive phase, is the first to undergo the physical reaction of melting in the process of thermal shock. The distribution of Zn in the center and the edge is very

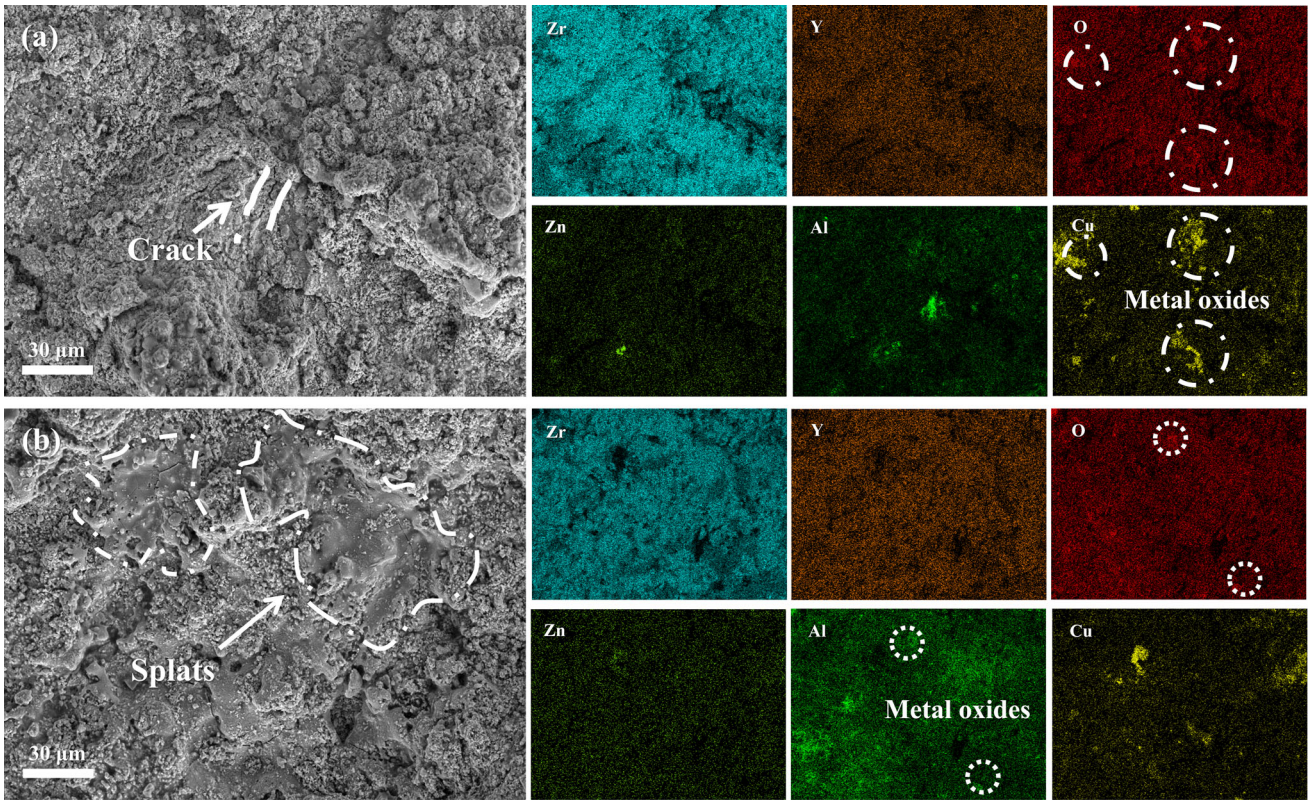

Fig. 9 S1 Surface morphology and elemental distribution after flame ablation (a) Center area of flame ablation; (b) Edge region of flame ablation

uniform, which shows that it has a significant effect on ablation. The oxidation is founded at all the positions of Al layers, and the newly generated oxides shows heat insulation. From Fig. 9, it can be seen that the oxidation products of Al are mostly concentrated in the edge region, which may attribute to the effect of erosion. Cu is in the center of the impact area of the presence of an oxidation phenomenon. The melting point of Cu is higher than the thermal shock temperature of the test, showing weak ablation effect obviously.

In order to further confirm the chemical composition changes of Al, Zn and Cu added to the coatings before and after flame ablation, the surface of the specimens before and after flame ablation is analyzed by XPS spectroscopy. Figure 10 shows the high-resolution XPS spectra of Al 2p, Cu 2p and Zn 2p of the coatings. Figure 10(a), and (b) shows that there are two characteristic peaks of Al and Al_2O_3 in the pristine coating. Their binding energies are 73.8 eV (Al) and 76.88 eV (Al_2O_3), and the ratio of their contents is 100:48 (Al: Al_2O_3). The characteristic peaks of Al and Al_2O_3 also existed on the surface of the ablated coating, and their binding energies were 74.08 eV (Al) and 77.59 eV (Al_2O_3), respectively, with a ratio of 100:54 (Al: Al_2O_3). As shown in Fig. 10(c), it can be seen that the Cu on the surface of the pristine coating existed in the state of metallic monomers with a binding energy of 923.66 eV. whereas after flame ablation, the main peak of CuO (with a binding energy of 934.94 eV) and the satellite peaks of CuO (with binding energies ranging from 945 eV to 940 eV) appeared with the ratio of the contents of the two at 100:41 (Cu: CuO). Analyzing Fig. 10(e), and (f) shows that there were two characteristic peaks of Zn and ZnO in the pristine coating. Their binding energies were 2021.5 eV (Zn) and 2022.2 eV (ZnO), and the ratio of their contents was 100:65 (Zn: ZnO). The characteristic peaks of Zn and ZnO also existed on the surface of the ablated coating, and their binding energies were 2021.5 eV (Zn) and 2022.2 eV (ZnO), respectively, with a ratio of 100:67 (Zn: ZnO). Combined with the elemental surface distribution of the coating, it can be concluded that the three metal additive phases of Al, Cu and Zn in the layer were mainly Al, Cu and Zn metal monomers, while at the same time encompassing a portion of Al_2O_3 and ZnO. After high-temperature ablation, the percentage of Al_2O_3 and ZnO content in the S1 coating did not change significantly. It was inferred that Al and Zn mainly undergo melting reactions at high temperatures. The newly generated product on the surface of the specimen after high-temperature ablation is CuO. Table 4 shows some of the thermal properties of Al, Zn and Cu (Ref 38). During the ablation process at 800 °C, Zn and Al melt and absorb heat successively, and Cu mainly undergoes an oxidation reaction before reaching the melting point. Therefore, the sweating and cooling of the S1 coating under the ablation condition of 800 °C mainly relies on Al and Zn (Ref 39). CuO in the oxidation product has an approximate thermal conductivity of ZrO2, which contributes to the overall thermal insulation of the coating (Ref 40), Al_2O_3 (Ref 41) and ZnO (Ref 42) have better antioxidant properties, which can mitigate the phenomenon of oxidative erosion of the coating as a whole, in addition to the better thermal stability of Al_2O_3 and ZnO at high temperatures (Ref 43).

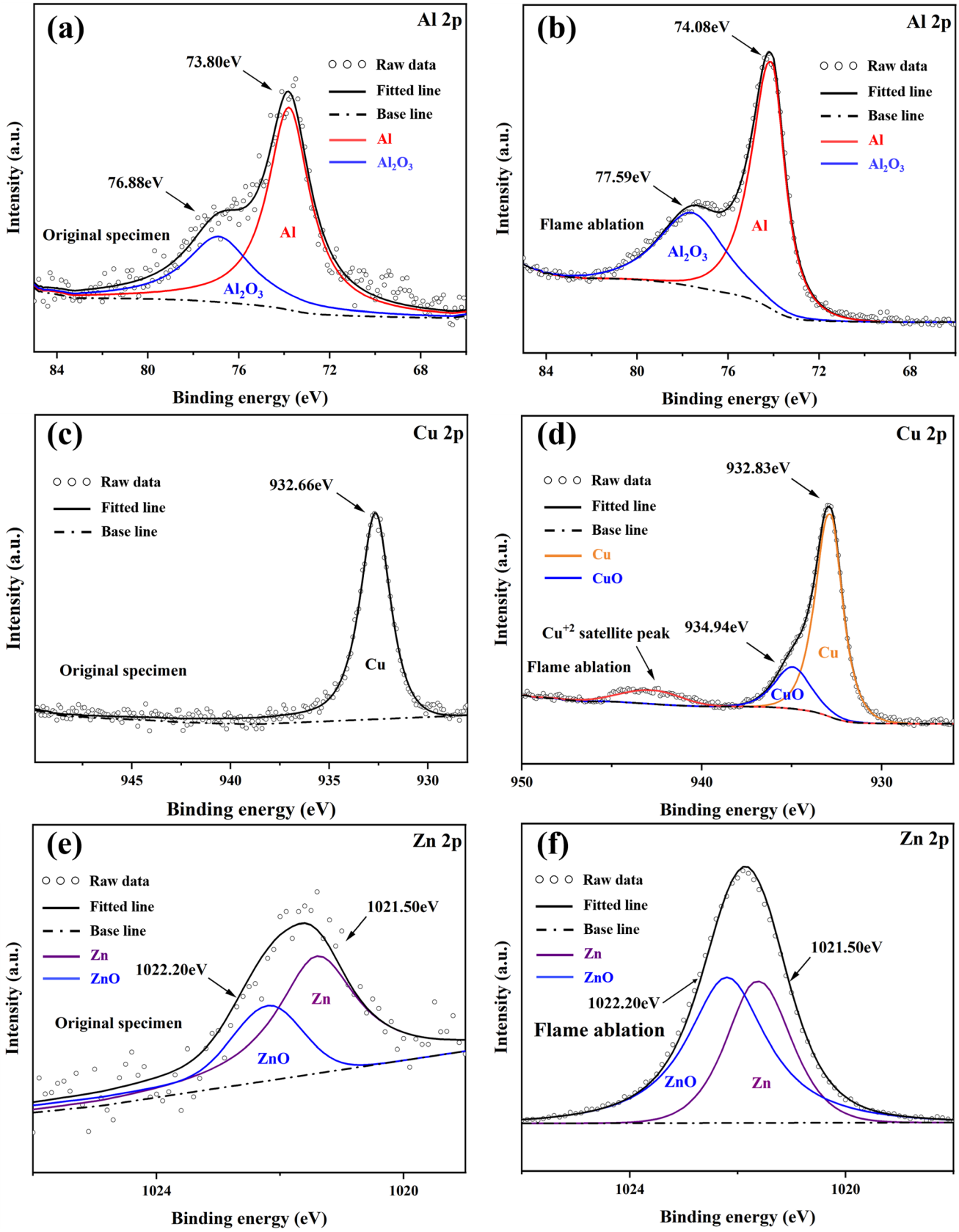

Fig. 10 (a) Fitting of Al 2p spectral peaks on the surface of the original specimen; (b) Fitting of Al 2p spectral peaks on flame-abraded surfaces; (c) Fitting of Cu 2p spectral peaks on the surface of the original specimen; (d) Fitting of Cu 2p spectral peaks on flame-abraded surfaces; (e) Fitting of Zn 2p spectral peaks on the surface of the original specimen; (f) Fitting of Zn 2p spectral peaks on flame-abraded surfaces

Table 4 Thermal properties of Al, Zn and Cu

	Melting point, °C	ΔHm, KJ mol^{-1}	Boiling point, °C	ΔHv, KJ mol^{-1}
Zn	420	7.32	907	123.6
Al	660	10.71	2327	294.0
Cu	1083	13.26	2835	300.4

4. Conclusion

In this experiment, YSZ composite coatings are prepared on resin-based composite substrates by the detonation spraying process. The influence of the addition phase on the thermal protection performance of the coating is discussed from the perspectives of phase, microstructure and ablation performance, as well as the ablation mechanisms of YSZ composite coatings are elaborated. The conclusions are summarized as follows:

(1) The detonation spraying process is able to prepare dense coatings with good interfacial bonding without damaging the resin matrix composites.
(2) Doping Al, Cu, and Zn in YSZ can reduce the infiltration of O during flame ablation and alleviate the cracking of the bottom layer.
(3) Under the high temperature ablation condition of 800°C, the Al and Zn additive phases play the role of melting and cooling, and the Al_2O_3, ZnO and CuO generated at high temperature play the role of heat insulation and repair coating.

Acknowledgments

This work was supported by the National Natural Science Foundation of China (52075508 and 52275194) and Jiangsu Province Postgraduate Practice Innovation Plan Project (SJCX23_1162).

Author contributions

BZ and HT conceived the idea of the study; YF, SZ and CF analyzed the data; BZ, HT and YF interpreted the results; all authors discussed the results and revised the manuscript.

Data Availability

The raw/processed data required to reproduce these findings cannot be shared at this time as the data also forms part of an ongoing study.

Competing interest

The authors declare that they have no known competing financial interests or personal relationships that could have appeared to influence the work reported in this paper.

References

1. C. Barile and C. Casavola, Mechanical Characterization of Carbon Fiber-Reinforced Plastic Specimens for Aerospace Applications, *Polym. Compos.*, 2019, **40**(2), p 716–722
2. C. Su, X. Wang, L. Ding, and P. Yu, Enhancement of Mechanical Behavior of Resin Matrices and Fiber Reinforced Polymer Composites by Incorporation of Multi-Wall Carbon Nanotubes, *Polym. Test.*, 2021, **96**, 107077
3. S. Kumarasamy, N.M. Mazlan, M.S.Z. Abidin, and A. Anjang, Influence of Fuel Absorption on the Mechanical Properties of Glass-Fiber-Reinforced Epoxy Laminates, *J. King Saud Univ. Eng. Sci.*, 2019, **32**(8), p 548–554
4. H. Ashrafizadeh, P. Mertiny, and A. Mcdonald, Determination of Temperature Distribution within Polyurethane Substrates During Deposition of Flame-Sprayed Aluminum-12silicon Coatings Using Green's Function Modeling and Experiments, *Surf. Coat. Technol.*, 2014, **259**, p 625–636
5. J. Ma, L. Shen, and Y. He, Application of Composite Materials in Engine, *Mater. Sci. Adv. Compos. Mater.*, 2017, **1**(1), p 32–40
6. B. Parveez, M.I. Kittur, I. Badruddin, S. Kamangar, M. Hussien, and M.A. Umarfarooq, Scientific Advancements in Composite Materials for Aircraft Applications: A Review, *Polymers*, 2022, **14**(22), p 5007
7. B.G. Falzon, and R. Pierce, Thermosetting Composite Materials in Aerostructures. Revolutionizing Aircraft Materials and Processes, pp. 57-86. (2020)
8. G. Chen, S. Zhu, Z. Jiang, L. Gao, Z. Ma, and L. Liu, Laser Ablation Protection of Polymer Matrix Composites by Adhesive Inorganic Coatings, *J. Mater. Sci.*, 2017, **52**(21), p 12734–12741
9. L. Brunnacker, *Short Carbon Fiber-Reinforced Thermoplastic Composites for Jet Engine Components*, Thesis, Lulea University of Technology, M.D, 2019
10. P.D. Mangalgiri, Polymer-Matrix Composites for High-Temperature Applications, *Def. Sci. J.*, 2005, **55**(2), p 175–193
11. R. Beydon, G. Bernhart, and Y. Segui, Measurement of Metallic Coatings Adesion to Fibre Reinfroced Plastic Materials, *Surf. Coat. Technol.*, 2000, **126**(1), p 39–47
12. P. Khatake, R. Taluja, M. Kumar, M. Reddy, F. Al-Ataby, S. Sood, and P. Sonia, Cold Spray Coating: A Review of Material Systems And Future Perspectives, *Mater. Today Proceed.*, 2023, **11**, p 015
13. S. Song, J. Yin, Y. Zhu, Y. Huang, X. Liu, and Z. Huang, Optical Coating on Cf/SiC Composites via Aqueous Slurry Painting and Reaction Bonding, *J. Inorg. Mater.*, 2017, **32**(2), p 210–214
14. D. Therrien, A. McDonald, and P. Mertiny, Temperature Measurements of Polymer Composite Flat Plates Coated with Aluminum-12silicon, International Thermal Spray Conference 2012 (Houston, TX), 2012, pp. 1-6
15. R. Gonzalez, H. Ashrafizadeh, A. Lopera, P. Mertiny, and A. Mcdonald, A Review of Thermal Spray Metallization of Polymer-Based Structures, *J. Therm. Spray Technol.*, 2016, **25**, p 897–919
16. H. Tian, C. Wang, M. Guo, Y. Cui, J. Gao, Z. Tang, Y. Liang, C. Song, H. Wang, G. Jin, and S. Wei, Study on Process And Performance of Thermal Protective Coating On Polyimide Resin Matrix Composite, *Ceram. Int.*, 2020, **46**(8), p 12744–12758
17. W. Huang, X. Fan, Z. Yu, Z. Xin, X. Meng, Y. Wang, B. Zou, X. Cao, and Z. Wang, Fabrication of Thermal Barrier Coatings onto Polyimide Matrix Composites via Air Plasma Spray Process, *Surf. Coat. Technol.*, 2012, **207**, p 421–429
18. P. Fauchais and G. Montavon, Thermal and Cold Spray: Recent Developments, *Key Eng. Mater.*, 2008, **4**(384), p 1–59
19. A. Liu, M. Guo, M. Zhao, H. Ma, and S. Hu, Arc Sprayed Erosion Resistant Coating for Carbon Fiber Reinforced Polymer Matrix Composite Substrates, *Surf. Coat. Technol.*, 2006, **200**(9), p 3073–3077
20. G. Sun, X. He, J. Jiang, and Y. Sun, Parametric Study of Al and Al2O3 Ceramic Coatings Deposited by Air Plasma Spray Onto Polymer Substrate, *Appl. Surf. Sci.*, 2011, **257**(17), p 7864–7870

21. A. Rezzoug, S. Abdi, N. Bouhelal, and I. Daoud, Metallic Coating for Carbon Fiber Reinforced Polymer Matrix Composite Substrate, *World Acad. Sci. Eng. Technol. Int. J. Chem. Mol. Nucl. Mater. Metall. Eng.*, 2016, **10**(1), p 64–69
22. Q. Peng, M. Liu, Y. Huang, G. Ma, W. Guo, H. Wang, and Z. Xing, Development Mechanism and Performance of Al2O3-PF Composite Coating on Epoxy Resin Matrix Composite Surface By Supersonic Plasma Spraying, *Surf. Coat. Technol.*, 2022, **446**(23), 128762
23. W. Huang, H. Cheng, C. Zhang, Y. Zhou, and X. Cao, Thermal Ablation of Stabilized Zirconia/Metal Coated Polyimide Matrix Composites Via Plasma Spray Process, *Plasma Chem. Plasma Process.*, 2015, **35**, p 587–603
24. H.R. Abedi, M. Salehi, and A. Shafyei, Microstructural, Mechanical and Thermal Shock Properties of Triple-Layer TBCs with Different Thicknesses of Bond Coat and Ceramic Top Coat Deposited Onto Polyimide Matrix Composite, *Ceram. Int.*, 2018, **44**(6), p 6212–6222
25. H.R. Abedi, M. Salehi, and A. Shafyei, Mechanical and Thermal Properties of Double-Layer and Triple-Layer Thermal Barrier Coatings with Different Ceramic Top Coats Onto Polyimide Matrix Composite, *Ceram. Int.*, 2017, **43**(15), p 12770–12780
26. J. Zhou, J. Jiang, L. Deng, J. Huang, J. Yuan, and X. Cao, Influence of Bond Coat on Thermal Shock Resistance and Thermal Ablation Resistance for Polymer Matrix Composites, *Front. Mater.*, 2021, **8**, 672617
27. H. Jeon, I. Lee, and Y. Oh, Changes in High-Temperature Thermal Properties of Modified YSZ with Various Rare Earth Doping Elements, *Ceram. Int.*, 2021, **48**(6), p 8177–8185
28. H.R. Abedi, M. Salehi, and A. Shafyei, Multi-Layered Thermal Barrier Coatings on BMI Polyimide Matrix Composite, *Surf. Coat. Technol.*, 2018, **337**(9), p 104–116
29. Y. Jia, H. Li, Q. Fu, and J. Sun, A ZrC-SiC/ZrC-LaB6/ZrC Multilayer Ablation Resistance Coating for SiC-Coated Carbon/Carbon Composites, *Surf. Coat. Technol.*, 2016, **309**, p 545–553
30. J. Chen, H. Yang, C. Xu, J. Cheng, and Y. Lu, Preparation of ZrO_2 Microspheres by Spray Granulation, *Powder Technol.*, 2021, **385**, p 234–241
31. B.A. Hunter, C.J. Howard, and D. Kim, Neutron Diffraction Study of Tetragonal Zirconias Containing Sn, *Physica B*, 1997, **241**, p 1249–1251
32. M. Matsuura, Y. Nishijima, N. Tezuka, S. Sugimoto, T. Shoji, and N. Sakuma, Increase of Energy Products of Zn-Bonded Sm-Fe-N Magnets with Low Oxygen Content, *J. Magn. Magn. Mater.*, 2018, **467**, p 64–68
33. H. Mahmoodi, M. Hadavi, and Y. Palizdar, Plasma Foil Aluminizing of Steel at a Temperature Below Aluminum Melting Point, *High Temp.*, 2023, **60**(5), p 599–606
34. B. Rakhadilov, D. Buitkenov, E. Kabdykenova, Z. Sagdoldina, and L.S. Zhurerova, Effect of the Detonation Spraying Mode on the Tribological Properties of NiCr-Al2O3 Coatings, *Eurasian J. Phys. Funct. Mater.*, 2021, **5**(1), p 39–44
35. J. Huang, W. Sun, R. Huang, and W. Ma, Cracking Behavior of Atmospheric Plasma-Sprayed 8YSZ Thermal Barrier Coatings during Thermal Shock Test, *Coatings*, 2023, **13**(2), p 243
36. S. Tao, J. Yang, W. Li, F. Shao, X. Zhong, H. Zhao, Y. Zhuang, J. Ni, S. Tao, and K. Yang, Thermal Stability of Plasma-Sprayed Thick Thermal Barrier Coatings Using Triplex ProTM-200 Torch, *Coatings*, 2020, **10**(9), p 894
37. Z. Wei, H. Cai, and C. Li, Comprehensive Dynamic Failure Mechanism of Thermal Barrier Coatings Based on a Novel Crack Propagation and TGO Growth Coupling Model, *Ceram. Int.*, 2018, **44**(18), p 22556–22566
38. J.A. Dean, *Lan's Handbook of Chemistry*, 2nd ed. Science Press, Beijing, 2003
39. Z. Zhao, K. Li, W. Li, Q. Liu, G. Kou, and Y. Zhang, Preparation, Ablation Behavior and Mechanism of C/C-ZrC-SiC and C/C-SiC Composites, *Ceram. Int.*, 2018, **44**(7), p 7481–7490
40. F. Bakkardouch, H. Atmani, M. Khalloufi, A. Jouaiti, and L. Laallam, Modified Cellulose-Based Hybrid Materials: Effect of ZnO and CuO Nanoparticles on the Thermal Insulation Property, *Mater. Chem. Phys.*, 2021, **271**(2), 124881
41. X. Zhang, Y. Wu, S. He, and D. Yang, Investigation on the Atomic Oxygen Erosion Resistance of Sol-Gel Alumina-Silica Composite Films on Kapton, *Mater. Chem. Phys.*, 2009, **114**(1), p 179–184
42. J. Wang, W. Li, Y. Chen, and L. Zhu, Anti-Atomic Oxygen Properties of Silicone Coating Modified by nano-ZnO, *J. Beijing Univ. Aeronaut. Astronaut*, 2009, **35**(7), p 824–827
43. X. Zhang, X. Zhuo, Z. Fan, J. Mao, C. Deng, C. Deng, X. Mei, J. Cui, K. Zhou, and M. Liu, Al2O3-Modified 7YSZ Thermal Barrier Coatings for Protection Against Volcanic ash Corrosion, *Npj Mater. Degrad.*, 2022, **6**(1), p 89